Heat Transfer and Cure in Pultrusion: Model and Experimental Verification

Gibson L. Batch and Christopher W. Macosko
Dept. of Chemical Engineering and Materials Science, University of Minnesota, Minneapolis, MN 55455

Though pultrusion has existed for nearly 40 years, factors affecting temperature and resin reactivity are not completely understood. A model is tested to help explain the effects of die temperature, line speed and initiator concentration on curing inside a pultrusion die. The model includes radio frequency preheating, heat conduction, heat of cure, changing thermal properties with temperature and degree of cure, and hindered heat transfer due to shrinkage of the profile away from the die. The analysis is compared to experimental temperature measurements for a 1-in. (25-mm) round die, where die temperature, line speed, and initiator concentration were varied. Temperature predictions by the model are in good agreement with the data for many of the conditions tested. Considerable disagreement still persists, however, under processing conditions with faster line speeds and lower die temperatures.

Introduction

Pultrusion is one of the few continuous processes for composites manufacture. In pultrusion (Figure 1), fiber reinforcements are saturated with resin and then continuously pulled through a heated die. Once inside the die, the resin cures and solidifies into a laminate with the same cross-sectional profile as the die. A puller continuously draws fibers through the die, and a traveling cutoff saw cuts the profiles into desired lengths. Unsaturated polyester resins are used most often in pultrusion applications, though vinyl ester and epoxy resins are used for enhanced physical properties and chemical resistance. Unidirectional fiberglass rovings are the most common reinforcement, with loadings from 50 to 70% by volume (67–83% by weight).

Since the inception of pultrusion in the mid-1950s, processors have made refinements to make products faster, of greater complexity, and of improved quality. For example, Goldsworthy (1971) has found that preheating the resin before entering the die will increase processing rates. However, pultrusion process variables—resin formulation, preheating temperature, die heater placement, and line speed—are still selected by operator experience. This is partly because pultrusion curing models are not available to the processors. If a model were available, however, it could help identify problems with misplaced heater bands, uneven die temperature, wall buildup or sloughing, and temporal changes in resin reactivity. Modeling performed on-line can help define process control strategies, such as whether to change a heater setting or line speed to most readily maintain product quality. Additionally, mathematical models can help troubleshoot new resin formulations.

This work describes a heat-transfer and cure model for pultrusion. The equations for heat transfer and reaction kinetics are solved numerically by finite differences. Unique features of this model are: 1) the kinetic equations based on the chemical mechanism of unsaturated polyester and vinyl ester resins; 2) changing physical properties during cure; 3) reduced heat-transfer rates due to skrinkage of the profile away from the die metal; and 4) allowances for a preheater. Temperature predictions inside the die are compared to experimental measurements using a vinyl ester resin cured in a 2.54-cm-dia. round die.

Previous Work

Previous works differ in the heat-transfer boundary conditions, the curing kinetic model, and the verification of the analysis. Price (1979) had the first pultrusion heat-transfer and cure model. The model was limited to either isothermal or adiabatic processing, neither of which was realistic for production. Also, variations in die temperature in the machine

Correspondence concerning this article should be addressed to G. L. Batch.
Present address of G. L. Batch: 3M Corporation, St. Paul, MN 55144.

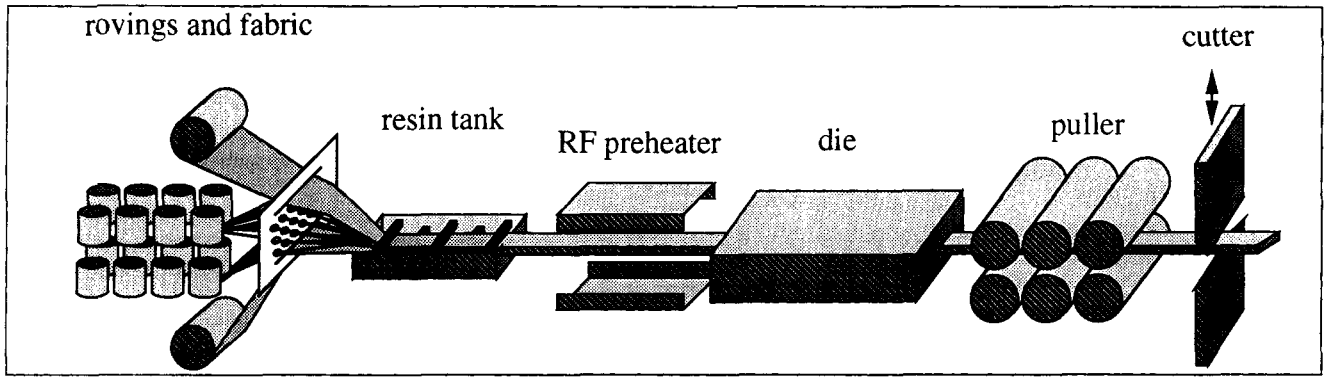

Figure 1. Pultrusion process schematic.

direction were neglected, and an empirical first-order model was used for curing kinetics. No experimental results were presented. Later, Aylward et al. (1985) repeated these calculations using the finite element method. Sumerak (1985) presents a descriptive model for pultrusion with experimental temperature and pressure data for a variety of resins and operating conditions. This model contained useful physical insight for processing, even though it was not quantitatively predictive. Roy (1986) analyzed the pultrusion of epoxies using first-order kinetics and a two-dimensional heat-transfer model for irregular geometries (such as I-beams). Langan (1986) used a lumped parameter model intended for process control calculations, though the model had considerable discrepancy with experimental temperature data for unsaturated polyester pultrusion. Ma et al. (1986) presented a heat-transfer analysis for epoxies which included axial conduction; however, no evidence was given to demonstrate that axial conduction was indeed significant. Tulig (1985) and later Buck et al. (1989) modeled the pultrusion using unique boundary conditions which simulated both the heat input from the heater bands outside the die and heat losses due to convection with air. Later, Walsh et al. (1988, 1989) and Gorthala et al. (1992) also analyzed the pultrusion of epoxy resins and included experimental verification. Trivisano et al. (1990) used a model for epoxy pultrusion to optimize the die temperature profile. Larock et al. (1989) and Astrom et al. (1991) derived a heat-transfer model for thermoplastic pultrusion using nonisothermal crystallization kinetic equations for heat released during cooling.

Most of the above work is for the pultrusion of epoxy resins, which have a small, but important, part of the total pultrusion production. Over 95% of the pultrusion market uses unsaturated polyester and vinyl ester resins, which has a different reaction chemistry and curing kinetics than epoxies. The pultrusion models by Batch and Macosko (1987), Han and Chin (1988), Buck et al. (1989), and Ng et al. (1989) used reaction kinetic models developed for unsaturated polyester resins. Though these kinetic models vary, they each had explicit predictions on the effect of inhibitor and initiator concentration on the rate of polymerization. In each of these works, however, the temperature predictions were not compared to experimental measurements. Because polyesters shrink more than epoxies during cure, Batch and Macosko added heat-transfer resistance as the profile shrinks away from the die. Later, Batch (1989, 1990a) experimentally verified models for temperature, resin pressure, and pulling force in pultrusion, and extended the analysis to include heat transfer through the die metal itself.

In this article, only the heat transfer and cure in the profile will be considered, and the metal die temperature is assumed known at several positions along the die length. Unlike previous articles, this work studies the effects of changing thermal properties, axial conduction, separation at the wall, and preheater settings on processing temperatures. Details of the model which are not reported here can be found in Batch (1989).

Model Formulation

Temperature profiles in a pultrusion die are shown in Figure 2. After leaving the resin tank, the resin and fibers may pass through a radio frequency (RF) preheater (Orfeuil, 1987; Jones, 1974). At the die entrance, there is a short taper section where excess resin is squeezed from the fibers. Once in the die, heat conducts from the die wall, so resin at the wall heats and gels before resin at the center. The reaction exotherm at the center can cause centerline temperature to exceed the temperature at the die wall. After polymerization is nearly complete, the solid composite shape shrinks away from the die as it cools to form an air gap. Evidence of this shrinkage can be seen in experimental pressure measurements (Sumerak, 1985), which show a sudden decrease in pressure after the maximum centerline temperature was reached.

The assumptions of the heat-transfer model are as follows.

1) The resin does not flow relative to the fibers in either longitudinal or transverse directions.

2) The heating rate inside the RF preheater is constant.

3) The die temperature is at steady state and a known function of position.

4) Longitudinal heat conduction through the resin and fibers is negligible.

5) The resin and fibers have the same local temperature.

6) Reaction rate is unaffected by chemical interactions with the fibers and fillers, or by internal resin pressure.

7) Frictional heat generation at the sliding metal/polymer interface along the perimeter of the profile is neglected.

These assumptions allow the composite to be modeled as a continuum, even though the fibers and resins are in distinct phases. Also, the reaction kinetic parameters determined by differential scanning calorimetry will be used directly in the analysis without modification for the presence of fillers and fiber, as supported by Ng et al. (1989). Because the resin layer between the fibers and the die wall is very thin (1–10 μm), the volume of drag-induced flow is negligible and hence the plug

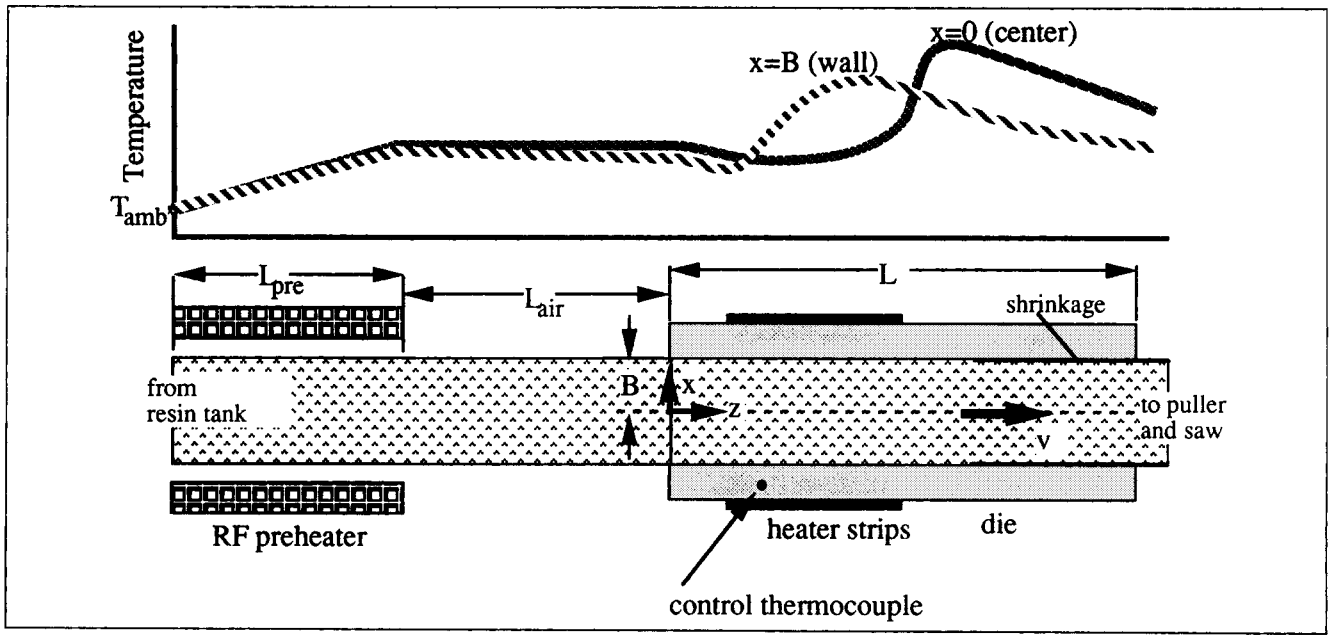

Figure 2. Pultrusion apparatus showing typical temperatures at the center and surface of the pultruded profile.
The profile thickness B was enlarged for clarity.

flow approximation is believed to be valid. The plug flow approximation is also supported by previous models (Batch, 1987, 1989), which found negligible resin flow relative to the fibers beyond short distances away from the entrance taper. The assumptions of negligible longitudinal heat conduction and frictional heating are discussed in Appendix B. Axial conduction is likely to be unimportant based on *a posteriori* calculations for heat flux. The temperature rise at the wall due to friction is calculated to be 6°C under ideal adiabatic conditions. It is unknown how much this temperature increase will affect curing rate. To the knowledge of the authors, models with coupled heat transfer and pulling force with frictional heating effects have not been published. Nevertheless, one can assume that frictional heating will become more important for higher line speeds due to a larger pulling force.

The geometry for the pultrusion model is in Figure 2. The equation of energy in the Lagrangian (material) frame of reference is:

$$\frac{\partial(\rho C T)}{\partial t} = \nabla \cdot (k \nabla T) + \Delta H_r \rho \frac{\partial X}{\partial t} \qquad (1)$$

transient = conduction + generation

where $\partial X/\partial t$ is the conversion rate of the reactive resin matrix, and ΔH_r is the heat released during cure per unit mass of the fiber/matrix composite. Neglecting longitudinal conduction and assuming that local changes in material properties are small, Eq. 1 simplifies as follows:

$$\frac{\partial T}{\partial t} = \alpha_{th} \frac{\partial^2 T}{\partial x^2} + \alpha_{th} \frac{G}{x} \frac{\partial T}{\partial x} + \Delta T_{ad} \frac{\partial X}{\partial t} \qquad (2)$$

where α_{th} is the thermal diffusivity ($=k/\rho\ C$), ΔT_{ad} is the adiabatic temperature rise ($=\Delta H_r/C$), and G is zero for flat profiles and unity for round profiles. Note that because the heat equation is expressed in the Lagrangian frame of reference, line speed v does not appear in Eq. 2 but instead affects the boundary conditions.

Boundary conditions

Boundary conditions define how the moving profiles interacts with the air and die. Convective boundary conditions are used:

$$\frac{\partial T}{\partial x}(B,z) = -\frac{Nu}{B}[T(B,z) - T_{die}(z)] \qquad (3)$$

where Nu is the Nusselt number ($=hB/k$), and T_{die} is the die metal temperature which changes with axial distance z. Initially, the resin is in good thermal contact with the die, so Nu is large. To reflect decreases in heat-transfer rate as the resin cures and shrinks away from the die, an empirical equation is used for Nu:

$$Nu = Nu_\infty \quad \text{for } S \geq 0$$
$$Nu = \frac{Nu_\infty}{1 - cS} \quad \text{for } S < 0 \qquad (4)$$

where S is the fractional change in volume based on the cross-sectional averaged temperature T_{avg} and degree of cure X_{avg}.

$$S \equiv a\,(T_{avg} - T_{amb}) - \gamma X_{avg} \qquad (5)$$

Thermal expansion coefficient a and shrinkage fraction γ reflect volumetric changes of the composite with temperature and cure, respectively. Because the resin at the wall cures before the center, shrinkage of resin near the wall is initially compensated by thermal expansion of resin heating in the center. Therefore, shrinkage of the profile away from the die surface

Table 1. Thermal Properties Models for Pultrusion Analysis

Density (g/cm^3):	
Neat resin	$\rho_o = \dfrac{\rho_i}{1-\gamma X + a(T-25)}$
Resin with clay filler	$\dfrac{1}{\rho_r} = \dfrac{1-w_{clay}}{\rho_o} + \dfrac{w_{clay}}{\rho_{clay}}$
Composite	$\dfrac{1}{\rho} = \dfrac{1-w_f}{\rho_r} + \dfrac{w_f}{\rho_f}$
Heat Capacity ($J/g\cdot°C$):	
Neat resin	$C_o = C_i + C_x X + C_l(T-25)$ for $T > T_g$ $C_o = C_i - C_g + C_x X + C_l(T-25)$ for $T < T_g$
Resin with clay filler	$C_r = (1-w_{clay})C_o + w_{clay}C_{clay}$
Composite	$C = (1-w_f)C_r + w_f C_f$
Thermal Conductivity ($W/cm\cdot°C$):	
Resin with clay filler	$k_r = k_{ri} + X[k_{rl}(T-25) + k_{rx}]$
Fibers	$k_f = k_{fi} + k_{fl}(T-25)$
Composite	$k = k_r \dfrac{1 + A B V_f}{1 - B V_f \Psi}$
where	$B = \dfrac{k_f/k_r - 1}{k_f/k_r + A}$ $\Psi = 1 + V_f \dfrac{1 - V_{max}}{V_{max}^2}$
Heat of Reaction (J/g):	
Resin with clay filler	$\Delta H_r = \Delta H_o(1 - w_{clay})$
Composite	$\Delta H_r = \Delta H_o(1 - w_{clay})(1 - w_f)$

depends on the density of the resin throughout the profile, and Eq. 5 uses an average temperature and conversion rather than simply the values near the die wall. The values of a and γ decrease with the addition of fibers and fillers in proportion to their volume fraction.

If the die temperature is uniform around the profile perimeter, then Eq. 2 will need to be solved for only half the profile thickness and the symmetric boundary condition will apply at the center:

$$\frac{\partial T}{\partial x}(0, z) = 0 \tag{6}$$

However, the analysis can be extended to include hollow sections by solving Eq. 2 throughout the cavity thickness, using Eq. 3 with different T_{die} and Nu for each surface.

Cooling outside the die can be modeled using an extension of the convective boundary condition:

$$\frac{\partial T}{\partial x}(B,z) = -\frac{Nu_{air}}{B}[T(B,z) - T_{amb}] \tag{7}$$

Air cooling will affect profile temperature in the preheater before the die. Modeling of the heat transfer beyond the die may also be important to insure that the composite is cooled sufficiently to prevent damage by the puller.

Initial conditions

Without a preheater, the initial temperature is the ambient temperature:

$$T(x,0) = T_{amb} \tag{8}$$

When a preheater is used, however, the heat-transfer and cure model is extended in front of the die. To approximate the temperature change in the preheater, Eq. 2 is modified as follows:

$$\frac{\partial T}{\partial t} = \vartheta(z)\,\alpha_{th}\frac{\partial^2 T}{\partial x^2} + \vartheta(z)\,\alpha_{th}\frac{G}{x}\frac{\partial T}{\partial x} + \Delta T_{ad}\frac{\partial X}{\partial t} + P(z) \tag{9}$$

where P is the rate of temperature rise while in the preheater, and ϑ is a relative decrease in thermal diffusivity ($0 < \vartheta < 1$) due to trapped air and excess resin between the fibers before entering the die. As the taper at the die entrance removes excess resin and air, ϑ approaches unity and Eq. 9 reduces to Eq. 2. Squeezing is assumed uniform across the thickness, so the resin temperature distribution will not change as the resin enters the die.

Thermal properties

Thermal properties of the resin—density, heat capacity, and thermal conductivity—change with temperature and cure (Kamal and Ryan, 1980; Pusatcioglu et al., 1979; Mijovic and Wang, 1988). Property models derived from a number of sources are summarized in Table 1. Additionally, fibers affect heat conduction in several ways:

As a Heat Sink. Fibers increase density and decrease heat capacity to increase the thermal mass ($\rho\ C$) of the composite.

As a Diluent. Fibers act as an inert filler which reduces the specific heat of reaction, ΔH_r.

As a Heat Conductor. Fibers increase thermal conductivity. Hence, composite density, heat capacity, and heat of reaction are based on the weight fractions of resin, filler and fiber. Composite thermal conductivity is based on the Lewis-Nielson equation (Ott, 1981; Progelhof et al., 1976).

Reaction kinetics

Unsaturated polyester and vinyl ester resins polymerize by the crosslinking free radical mechanism. Several workers (Lee, 1981; Gonzalez, 1983; Stevenson, 1986; Batch, 1989; Batch and Macosko, 1990b, 1992) have developed kinetic models based on the mechanisms of free radical initiation, radical inhibition and chain propagation. The following kinetic model (Batch and Macosko, 1992) is useful for composites processing because it predicts: 1) the effect of variable initiator and inhibitor concentrations on resin reactivity; 2) diffusion-limited propagation and incomplete cure due to vitrification.

Propagation:

$$\frac{\partial X}{\partial t} = k_p F_{active}[R]_{tot}(1 - X) \tag{10}$$

Initiator consumption:

$$\frac{\partial I_i}{\partial t} = k_{d,i}(1 - I_i) \tag{11}$$

Radical formation:

$$\frac{\partial [R]_{\text{tot}}}{\partial t} = \sum_j 2 f k_{d,j}(1 - I_j)[I]_{o,j} - k_z [R]_{\text{tot}}[Z]_{\text{eff}}(1 - Z) \tag{12}$$

Inhibitor consumption:

$$\frac{\partial Z}{\partial t} = k_z [R]_{\text{tot}} \frac{[I]_o - [I]_1}{[I]_o}(1 - Z) \tag{13}$$

The kinetic model has four independent variables—the total radical concentration $[R]_{\text{tot}}$ and the conversions of double bonds X, initiator, I, and inhibitor, Z.

$$X(t) \equiv \frac{[M]_o - [M](t)}{[M]_o}, \quad I(t) \equiv \frac{[I]_o - [I](t)}{[I]_o},$$

$$Z(t) \equiv \frac{[Z]_o - [Z](t)}{[Z]_o}$$

The three rate constants are assumed to have Arrhenius temperature dependence, $k_\iota = A_\iota \exp(-E_\iota/RT)$ where $\iota = d$, z, or p. The initiator efficiency f is empirically assumed to decrease from f_1 to f_2 between monomer conversions X_D and X_f to model the cage effect at high cross-link density:

$$\begin{aligned} f &= f_1 && \text{for } X < X_D \\ f &= f_1 - (f_1 - f_2)\frac{X - X_D}{X_f - X_D} && \text{for } X_D < X < X_f \\ f &= f_2 && \text{for } X > X_f \end{aligned} \tag{14}$$

Also due to the cage effect, not all the free radicals will be available for propagation. For monomer conversions above X_f, the active radical concentration F_{active} has been observed to linearly decrease for several crosslinking systems (Batch and Macosko, 1992):

$$\begin{aligned} F_{\text{active}} &= 1 && \text{for } X < X_f \\ F_{\text{active}} &= \frac{X_{\max} - X}{X_{\max} - X_f} && \text{for } X \geq X_f \end{aligned} \tag{15}$$

The maximum degree of cure $X_{\max}$ depends on reaction temperature. Residual monomer in the resin after processing can be removed either by post-curing to temperatures above the glass transition temperature (hence, letting X_{max} approach unity) or by slow diffusion of monomer to the atmosphere.

The numerical technique for solving the above equations for temperature and reaction kinetics are discussed in Appendix A. Experimental techniques for verifying predictions of the model are discussed next.

Experimental Techniques

Pultrusion experiments were performed on a 1-in. (25-mm) round die at the Dow Chemical Company (Freeport, TX) on a machine manufactured by Morrison Molded Fiberglass (Model TM570). Resin and fibers were RF preheated before entering the die. The die was 48 in. (122 cm) long and had 1,000-W strip heaters mounted on the four lateral external surfaces between 21 cm and 61 cm from the die entrance. The remainder of the die was unheated and uninsulated. A vinyl ester resin (Dow Derakane 411-35LI) was used with 15 parts per hundred (phr) resin ASP400 clay filler and 1 phr mold release (Ortholeum 162, Dupont). The initiator was tertbutyl peroctoate (TBPO) (Trigonox 21, Noury Chemical) at concentrations of both 1 and 2 phr. The glass reinforcement (Owens Corning OCF113) was at 62.4% by volume or 79% by weight.

Table 2. Operating Conditions for Pultrusion Experiments

Run	1	2	3	4	5	6
Initiator Conc. (phr)	1	1	2	1	1	2
$[I]_o$ (mM)	56.8	56.8	113.6	56.8	56.8	113.6
v (cm/s)	0.505	0.505	0.505	0.954	0.505	1.006
Die cntl. temp. (°C)	135	124	125	134	99	145
T_{pre} (°C)	84	84	73	64	79	53
P (°C/s)	0.48	0.48	0.40	0.61	0.44	0.49
T_{die} (°C)						
@ 0 cm	58.6	57.6	50.8	47.7	55.8	40.3
@ 12 cm	84.4	79.8	76.8	75.9	71.1	75.1
@ 24 cm	114.9	106.0	106.4	110.6	88.5	117.1
@ 36 cm	144.9	133.0	135.8	147.2	105.0	160.4
@ 48 cm	149.0	137.0	141.9	157.1	108.0	171.1
@ 60 cm	128.1	119.0	122.7	137.9	95.9	147.8
@ 72 cm	106.4	100.5	102.4	114.4	82.6	121.2
@ 84 cm	97.4	92.6	92.3	103.0	76.4	106.6
@ 96 cm	92.9	88.6	89.2	96.9	73.2	100.6
@ 108 cm	89.1	85.2	84.2	92.1	70.7	94.0
@ 122 cm	85.2	82.1	77.7	87.3	68.3	86.3

Operating conditions for the pultrusion experiments are summarized in Table 2. The experiments had several die temperatures T_{sp} (at location shown in Figure 2) and preheat temperatures T_{pre}. For each condition, thermocouples inside the die block measured temperature at ten locations after steady-state die temperature was achieved (approximately an hour after a change in set point). The die temperatures in Table 2 were found by interpolating between these measured temperature locations to points on regular 12-cm intervals.

Profile temperatures were measured by feeding long welded Type J thermocouple wires [0.01-in.-dia. (0.25-mm-dia.), 0.01-s response time] between fibers at the die entrance. Axial position was determined by multiplying line speed by the time elapsed since the entry into the die. Similar experiments were conducted by Jones (1974), Sumerak (1985), and Sumerak and Martin (1986). The radial position of each thermocouple was determined by sectioning the profile after cure. The uncertainty in measured temperature is ±5°C, in axial position is ±5 cm, and in radial position is ±0.1 cm (Batch, 1989).

Results and Discussion

Contour plots of the model predictions of temperature, conversion, and inhibitor conversion for run 1 are in Figures 3a–3c. Even though the heating from the RF Preheater is uniform, the temperature at the die entrance is nonuniform due to heat losses to the air. Once inside the die, heat conduction to the profile depletes the inhibitor at the perimeter before the center.

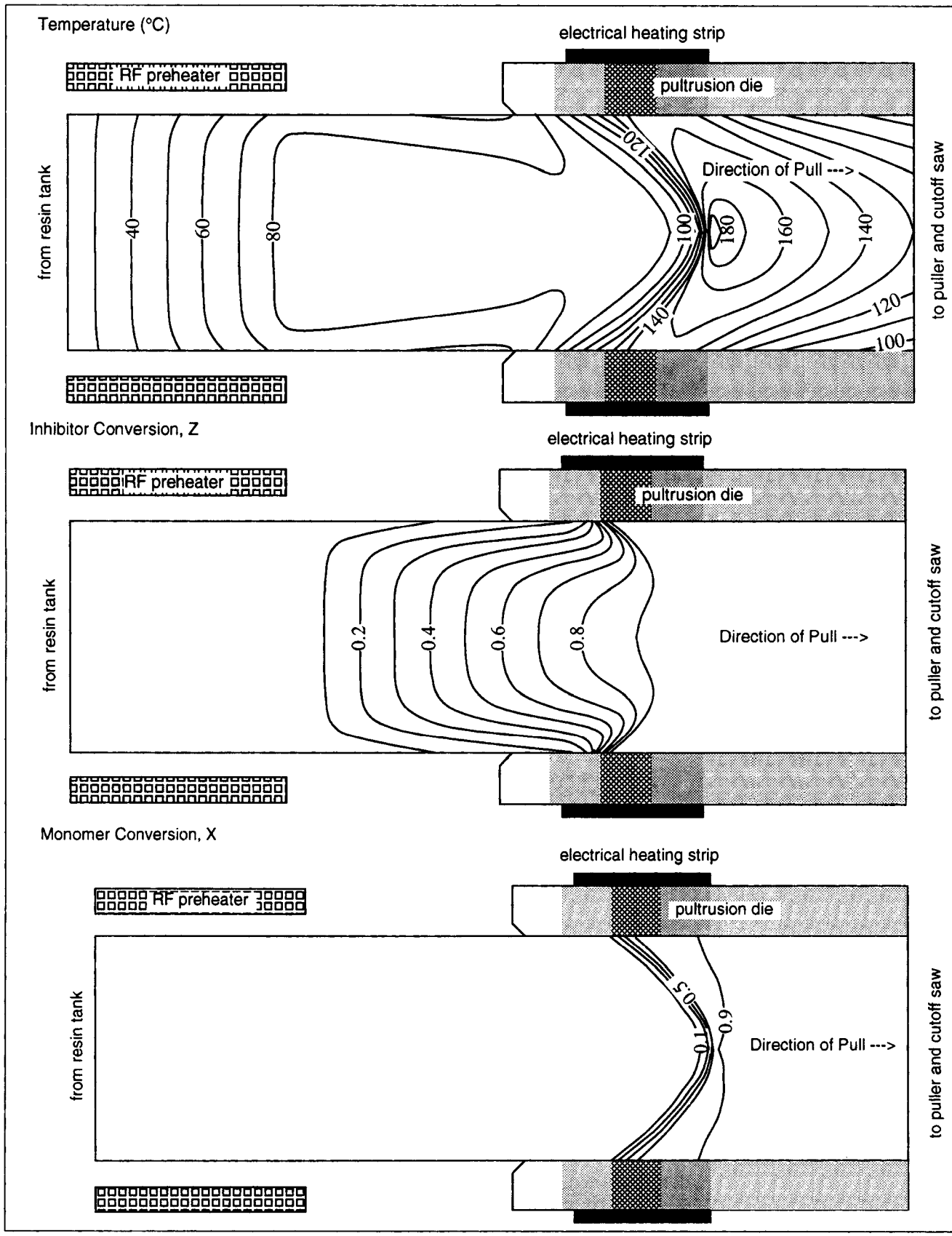

Figure 3. Predicted results for run 1 as the profile moves from the preheater (top) to the end (bottom) of the die: a) temperature; b) inhibitor conversion; c) monomer conversion.

The profile width is increased 60 times relative to its length for clarity. The pultrusion die is shaded to reflect temperature.

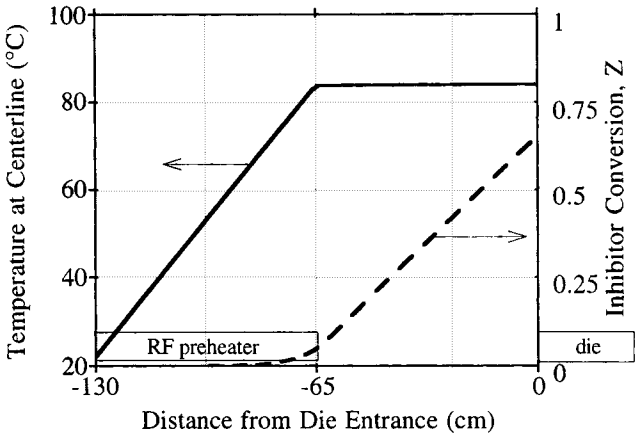

Figure 4. Resin temperature and inhibitor conversion as the profile passes through the preheater and air space before die entrance.

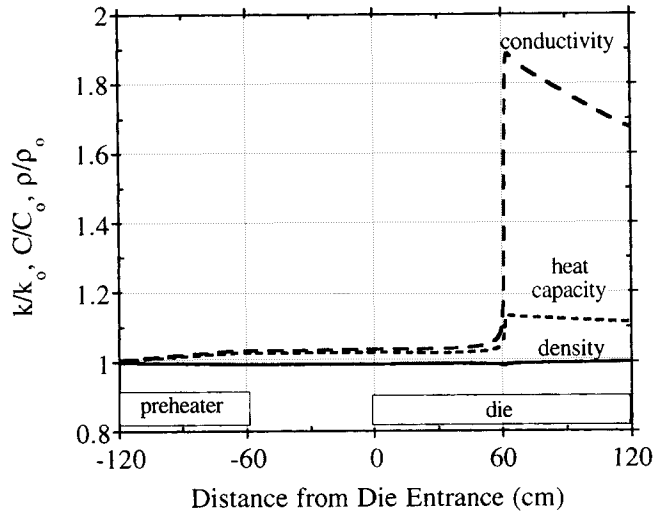

Figure 5. Predicted changes of thermal properties during pultrusion relative to their uncured values at room temperature.

The cross-linking polymerization begins shortly after all the inhibitor is consumed at the die wall. Thermal acceleration by the reaction exotherm drives the reaction rapidly to the center of the profile. After the peak exotherm in the center, temperature rapidly decreases due to conduction to the die wall. Hence, though heat conducts from the wall to the profile to initiate polymerization near the die entrance, it conducts in the opposite direction later in the die during cooling.

Sensitivity analysis

Before comparing the calculated temperatures to experimental values, the sensitivity of temperature predictions to various model input parameters is examined. A discussion of numerical errors due to truncation errors and axial conduction is in Appendix B. The discussion here will cover inhibitor consumption during preheating, changes in thermal properties with temperature and cure, and retardation of cooling due to shrinkage inside the die.

Inhibitor Consumption and Premature Gelation. The preheater affects both temperature and inhibitor concentration before the die (Figure 4). Temperature increases linearly through the preheater, as expected from Eq. 9 when P is constant. Between the preheater and die, however, where temperature is greatest, the inhibitor conversion increases substantially. Hence, resin temperature is proportional to residence time in the preheater, and inhibitor conversion increases with residence time between the preheater and die entrance. The rate of radical initiation (Eqs. 11 and 12) increases exponentially with temperature, so inhibitor consumption is very temperature-sensitive.

Because vinyl ester and polyester resins gel shortly after inhibitor consumption (Yang and Lee, 1988; Gonzalez-Romero and Macosko, 1985), conditions which have inhibitor conversion approaching unity before the die should be avoided. To decrease the risk of premature gelation, one can 1) reduce the preheater temperature, 2) move the preheater closer to the die entrance, or 3) add more inhibitor to the formulation. Addition of inhibitor to a resin is not practical for many processors. Most often the preheater temperature is reduced. The decreased reactivity from lower temperatures is offset by either higher die temperatures or slower line speeds. By moving the preheater closer to the die, however, the risk of premature gelation is reduced without sacrificing either preheater temperature or line speed. Moving the preheater simply decreases the time that the resin must endure ungelled before squeezing through the die entrance.

Thermal Properties. Resin density, thermal conductivity, and heat capacity will change with temperature and extent of cure. Density decreases with thermal expansion then increases again due to shrinkage, though as shown in Figure 5 the overall change is less than 2%. In contrast, heat capacity increases by 13% during cure, and thermal conductivity increases by nearly 90%. The net effect of these property changes is a 68% increase in thermal diffusivity and a 12% decrease in adiabatic temperature rise. A comparison of centerline predictions with and without changing properties is in Figure 6. The predicted temperatures after polymerization are 15°C lower, when changing thermal properties are added to the model. These lower temperatures will affect predictions for warp, residual shrinkage stress and surface quality (Batch, 1990c) and pulling force (Batch, 1989). They will also affect the separation boundary conditions, as discussed next.

Shrinkage Away from Die. The separation of the profile from the die will reduce the cooling rate. Initially, the resin is in compression due to backflow resistance through the die entrance (Batch, 1990c, 1989). Heating causes an additional pressure rise as resin attempts to expand in a confined cross-sectional area of the die. However, polymerization will increase density and reduce die pressure, until the profile eventually shrinks away from the die wall.

Effects of the resulting air gap on heat transfer have been modeled empirically by decreasing the wall Nusselt number Nu whenever the cross-sectional area of the profile is less than the die opening (Eq. 4). Figure 7 shows the predicted changes in Nu and volumetric change S as a function of distance through the die for run 1. Under these conditions, the point of separation (52 cm) is close to the peak exotherm (49 cm). Before the point of separation, Nu is some large value, Nu_∞, and S is positive indicating that the resin is thermally expanding to compress against the die profile. As curing shrinkage coun-

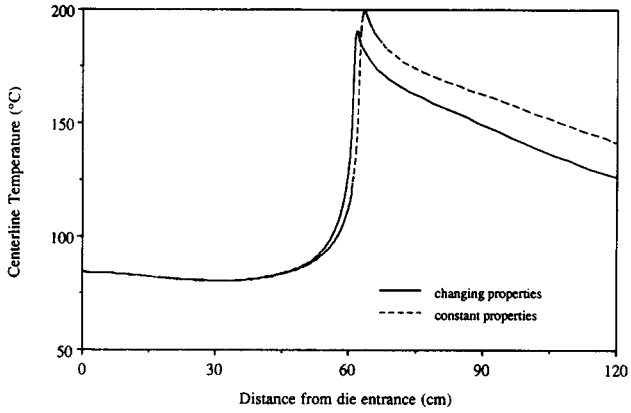

Figure 6. Effect of changing thermal properties on temperature predictions for run 1.

teracts thermal expansion, S is negative and Nu decreases. Note that a short distance away from the point of shrinkage that Nu drops over 60%, hindering heat transfer during cooling. The effect of decreasing Nu on heat transfer is seen in Figure 8, where the predictions with $c=0$ have uniform heat transfer throughout the die ($Nu=Nu_\infty$) and with $c=150$ have changes in Nu according to Eq. 4, as shown in Figure 7. The agreement between the model and experimental data is quite good when $c=150$ and Nu_∞ is 40. These same parameters are used in all the predicted temperature profiles shown below.

Experimental validation

Experimental and predicted temperatures near the centerline and wall are in Figures 9–14. All input parameters are listed in Tables 2 and 3. Kinetic parameters are determined by isothermal differential scanning calorimetry (Batch and Macosko, 1992; Batch, 1989), taking care to remove oxygen from the headspace of the sample pan (Batch and Macosko, 1990d). Other parameters are found as noted. The predictions at the wall and center are plotted for nodes closest to the experimental radial location of each thermocouple. Comparisons between the data and model are based on three criteria: 1) the location of the peak temperature near the center, 2) the magnitude of

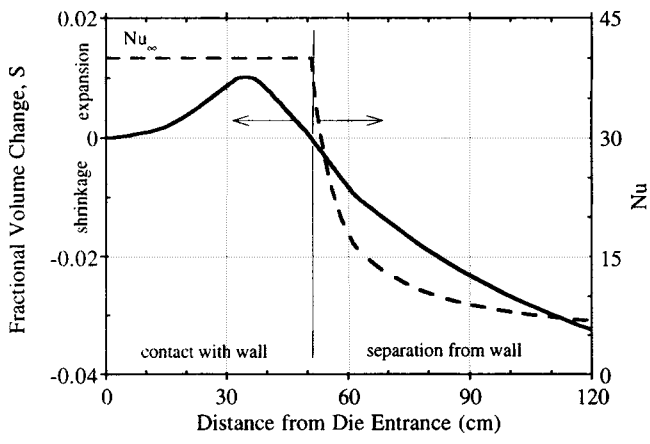

Figure 7. Changes in fractional volume change *S* and Nusselt number *Nu* as the profile cures and shrinks away from the die.

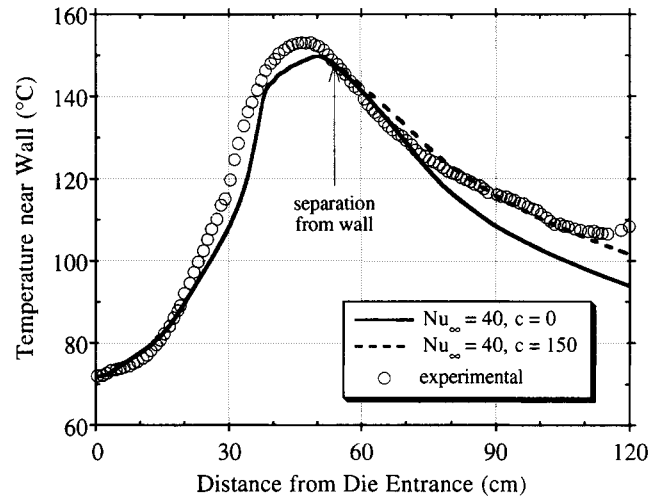

Figure 8. Effect of heat-transfer boundary conditions on predicted temperature near the wall compared to experimental data for run 1.

peak temperature, and 3) qualitative agreement over the length of the die. A summary of comparisons is in Table 4.

The agreement between predicted and experimental temperatures is excellent for runs 1 and 2 (Figures 9 and 10). The peak centerline temperature T_{max} and peak location z_{max} are predicted within experimental uncertainty of the observed data, and the temperatures along the entire length of the die are in good qualitative agreement.

Run 3 (Figure 11) tests the model when the initiator concentration is doubled while maintaining nearly the same operating conditions as in run 2. The location of the reaction exotherm agrees with the data, though the calculated peak temperature is higher than observed experimentally. The cooling rate after the exotherm is underpredicted at both the wall and center locations, possibly as a result of premature wall separation due to sloughing in the experiments.

In runs 4, 5 and 6 (Figures 12, 13 and 14, respectively), the predicted *wall* temperatures are in good agreement with the data, indicating that the boundary conditions were correct (that

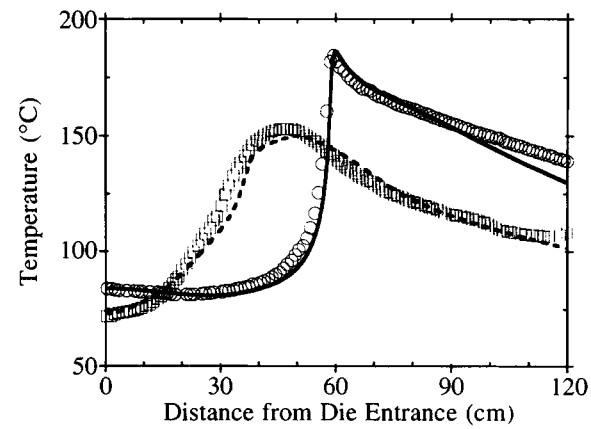

Figure 9. Comparison of predicted and experimental temperatures for run 1.

Circles are experimental data near the center ($r=0.07$ cm), squares are data near the wall ($r=1.14$ cm), and solid and dashed lines are predictions at nodes close to those respective radial locations.

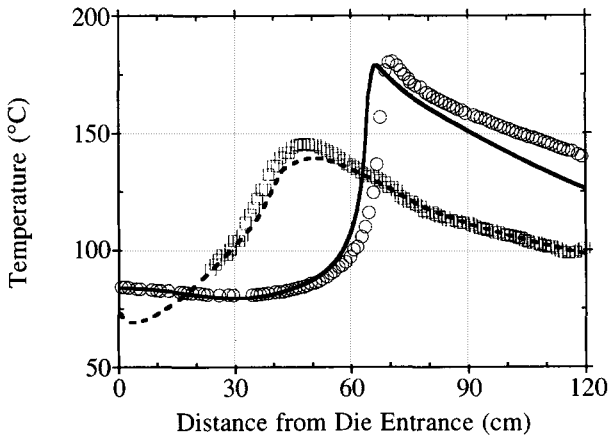

Figure 10. Comparison of predicted and experimental temperatures for run 2.

The same symbols as in Figure 9 were used. Experimental data near center and wall are at $r = 0.15$ cm and $r = 1.11$ cm, respectively.

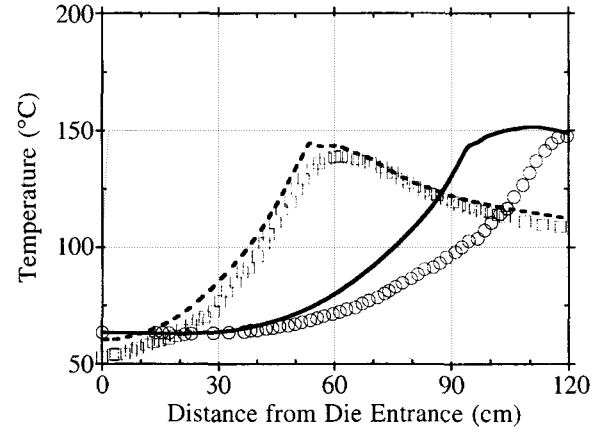

Figure 12. Comparison of predicted and experimental temperatures for run 4.

The same symbols as in Figure 9 were used. Experimental data near center and wall are at $r = 0.45$ cm and $r = 1.02$ cm, respectively.

is, frictional heating can be neglected). Yet in runs 4 and 6, the model predicted a faster reaction at the center than observed experimentally, and in run 5 the exotherm is predicted too late. Given the temperature agreement at the wall, the centerline discrepancy in runs 4-6 suggest that the reaction kinetics are incorrect. Uncontrolled factors which can affect the reaction kinetics are dissolved oxygen, fluctuations in preheater power, resin aging, and poor resin mixing. It is interesting to note that the model is most accurate (runs 1, 2 and 3) when the peak exotherm is close to the heater bands. In contrast, when the peak exotherm is away from the heater bands, centerline temperatures are in greatest error. It is possible that the model would be in better agreement with the data at higher line speeds, if the heater bands were moved closer to the die exit. More experimental work is necessary to prove this out.

Conclusions

A mathematical model for heat transfer and cure inside a pultrusion die was developed to include the effects of RF preheating before the die, changes in thermal properties with temperature and degree of cure, hindered cooling due to separation of the profile away from the die wall, and air cooling of the profile while outside the die. The equations of transient one-dimensional heat transfer and reaction kinetics were solved by implicit finite differences. Predicted temperatures were compared to experimental data for a round profile under a variety of processing conditions. The model accurately predicted temperature for changes in die temperature and initiator concentration at low line speeds. The wall temperatures were also accurately predicted at higher line speeds, though the centerline temperatures had considerable discrepancy. Under these conditions, the peak exotherm was down line from the heater bands, perhaps making the cure sensitive to uncontrolled factors such as dissolved oxygen, resin aging, fluctuations in preheater power, and poor resin mixing.

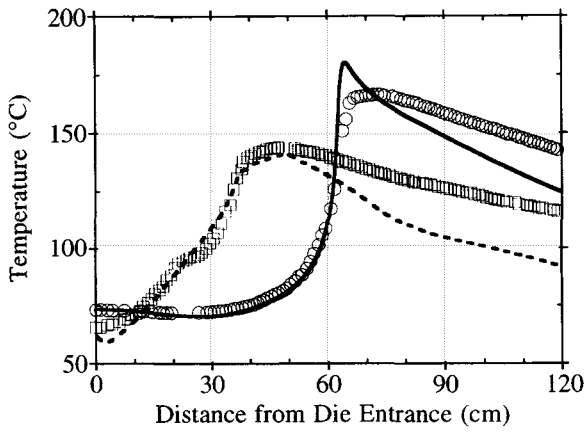

Figure 11. Comparison of predicted and experimental temperatures for run 3.

The same symbols as in Figure 9 were used. Experimental data near center and wall are at $r = 0.18$ cm and $r = 1.20$ cm, respectively.

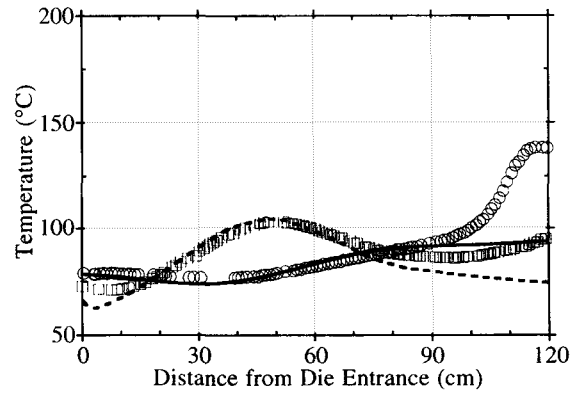

Figure 13. Comparison of predicted and experimental temperatures for run 5.

The same symbols as in Figure 9 were used. Experimental data near center and wall are at $r = 0.28$ cm and $r = 1.17$ cm, respectively.

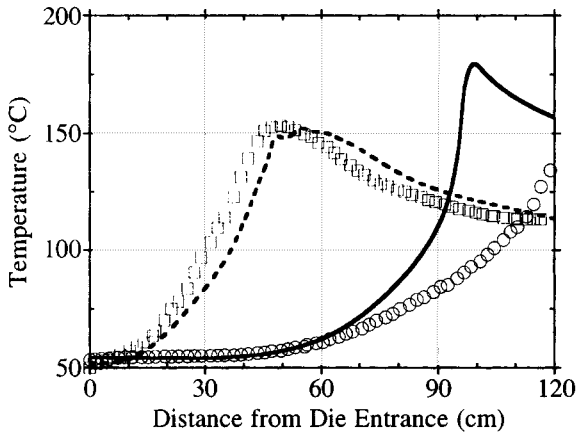

Figure 14. Comparison of predicted and experimental temperatures for run 6.

The same symbols as in Figure 9 were used. Experimental data near center and wall are at $r = 0.18$ cm and $r = 1.06$ cm, respectively.

Acknowledgment

The authors gratefully acknowledge Larry Blankenship, James Barren, H. Jay Buck, and Paul Byron of the Dow Chemical Company (Freeport, Texas) for the pultrusion data used in this work. Financial support was provided by the Pultrusion Technology, Inc. (Twinsburg, OH), Alcoa (Pittsburgh, PA), W. H. Brady Co. (Milwaukee, WI), the Minnesota Supercomputer Institute, the Minnesota Productivity Center, and the Graduate School of the University of Minnesota. GLB also thanks 3M Corporation for allowing time to finish this article.

Notation

a = volumetric thermal expansion coefficient
B = profile radius or half thickness, cm
c = empirical constant for changes in Nu with shrinkage
C = heat capacity, J/g·K
E_x = maximum allowable iteration update for conversion
E_T = maximum allowable iteration update for temperature
f = initiation efficiency
F = rate of heat conduction, K/s
F_{active} = fraction of active radicals for crosslinking
G = geometric factor (= 0 for rectangular, = 1 for cylindrical)
ΔH_r = specific heat of reaction, J/g
I = initiator conversion
$[I]_o$ = initial initiator concentration, mol/L
$[I]_1$ = empirical initiator concentration correction term, mol/L
k = thermal conductivity, W/cm·K
k_d = rate constant for initiation, s^{-1}
k_p = rate constant for propagation, l/mol·s
k_z = rate constant for inhibition, l/mol·s
$K_{i,t}$ = rate of heat conduction at node i and time t, K/s
L_{pre} = length of RF preheater, cm

Table 3. Parameters for Heat-Transfer Calculations*

Numerical Iteration Parameters:		
N	17	
Δt_{max}	5 s	
Δt_{min}	0.5 s	
ϵ_{toler}	0.001	
E_x	0.1	
E_T	0.1°C	
R	1.3	
Thermal Properties:		
ρ_i	1.04 g/cm³	Anderson and Messick, 1980, p. 37
γ	0.047	Lubin, 1982, p. 46
a	0.00052°C^{-1}	correlated to die shrinkage location
ρ_{clay}	2.6 g/cm³	Meyer, 1985, p. 73
ρ_f	2.56 g/cm³	Lubin, 1982, p. 140
C_i	1.715 J/g·°C	adiabatic reaction calorimetry
C_x	0.294 J/g·°C	room temperature calorimetry
C_t	0.0025 J/g·(°C)²	Mijovic and Wang, 1988
C_g	0.29 J/g·°C	DSC measurements, 10 K/min
C_{clay}	0.92 J/g·°C	Perry and Chilton, 1973, p. 3
C_f	0.67 J/g·°C	Perry and Chilton, 1973, p. 3
k_{ri}	1.22×10^{-3} W/cm·°C	transient temperature measurements
k_{rt}	1.47×10^{-5} W/cm·(°C)²	Pusacioglu et al., 1979
k_{rx}	6.1×10^{-4} W/cm·°C	assumed $k_{ri}/2$ according to Pusacioglu, 1979
k_{fi}	11.1×10^{-3} W/cm·°C	Weast, 1978, p. E6
k_{ft}	1.9×10^{-5} W/cm·(°C)²	Weast, 1978, p. E6
A	0.5	Ott, 1981; Progelhof et al., 1976
V_{max}	0.82	Ott, 1981; Progelhof et al., 1976
ΔH_o	325 J/g	DSC neat resin @ 10 K/min

* For details of experimental procedures, see Batch (1989) or references as indicated.

*Kinetic Parameters***:		
A_d	4.03×10^{14} s^{-1}	TPBO initiator
E_d	130.15 kJ/mol	
f_1	0.6	estimated before diffusion limitations
f_2	0.1	estimated after diffusion limitations
$[I]_1$	15.4 mM	
$[Z]_{eff}$	0.84 mM	
A_p	6.61×10^5 l/mol·s	
E_p	35.14 kJ/mol	
X_D	0.20	
X_f	0.32	
X_{max}	0.94	estimated from adiabatic temperature rise
k_z/k_p	150	
Operating Conditions:		
T_{amb}	22°C	
L_{pre}	65 cm	
L_{air}	65 cm	
P	see Table 2	fit to temperature profile at die entrance
ϑ	0.15	fit to temperature profile at die entrance
Nu_{air}	1.2	fit to temperature profile at die entrance
v	see Table 2	
B	1.27 cm	
L	121.9 cm	
G	1	round profile
Nu_∞	40	fit to die and profile temperatures from run 1
c	150	fit to die and profile temperatures from run 1
$T_{die}(x)$	see Table 2	interpolated from experimental locations
w_{clay}	0.13	
V_f	0.624	
w_f	0.79	

** Fit to isothermal DSC data (Batch and Macosko, 1992).

Table 4. Comparison between Predictions and Experiments

Run	Experimental T_{max}(°C)	Experimental z_{max}(cm)	Predicted T_{max}(°C)	Predicted z_{max}(cm)	Fit Quality
1	185±5	59±5	187	60	excellent
2	181±5	71±5	187	66	excellent
3	167±5	73±5	181	65	good
4	150±5	136±5	152	110	good
5	138±5	120±5	*	*	poor
6	160±5	131±5	180	99	poor

* No peak exotherm observed inside die.

L_{air} = distance between preheater and die entrance, cm
L = die length, cm
Nu_{air} = Nusselt number for profile heat transfer to air ($=h_{air}B/k$)
Nu = Nusselt number for profile heat transfer to die ($=h_{die}B/k$)
Nu_{∞} = Nusselt number before shrinkage
P = rate of temperature increase inside RF preheater, K/s
Pe = Peclet number vL/α_{th}
R = maximum allowable relative change in time step size
$[R]_{tot}$ = total concentration of initiated radicals, l/mol
S = shrinkage fraction
t = time, s
Δt_{max} = maximum time step size, s
Δt_{min} = minimum time step size, s
ΔT_{ad} = adiabatic temperature rise ($=\Delta H_r/C$), K
T = temperature, K
T_{amb} = ambient air temperature, K
T_{die} = die temperature at profile/die interface, K
v = line speed, cm/s
V_f = fiber volume fraction
w_{clay}, w_f = weight fraction clay and fiber
x = transverse coordinate, distance from centerline, cm
X = monomer conversion
z = longitudinal coordinate, distance from die entrance, cm
Z = inhibitor conversion

Greek letters

α_{th} = thermal diffusivity, cm^2/s
ϵ_{toler} = maximum allowable local truncation error
ϵ = local truncation error
γ = shrinkage fraction during cure
ϑ = insulation factor for air between fibers during preheating
ρ = density, g/cm^3

Literature Cited

Anderson, T. F., and V. B. Messick, "Vinyl Ester Resins," *Developments in Reinforced Plastics*, Elsevier Applied Science, New York (1980).

Åstrom, B. T., and R. B. Pipes, "Modeling of a Thermoplastic Pultrusion Process," *SAMPE Quarterly*, **22**(4), 55 (1991).

Aylward, L., C. Douglas, and D. Roylance, "A Transient Finite Element Model for Pultrusion Processing," *Poly. Proc. Eng.*, **3**, 247 (1985).

Batch, G. L., and C. W. Macosko, "A Computer Analysis of Temperature and Pressure Distributions in a Pultrusion Die," Conf. Compos. Inst. Soc. Plast. Ind., 12-B (1987).

Batch, G. L., "Crosslinking Free Radical Kinetics and the Pultrusion Processing of Composites," PhD Thesis, Univ. of Minnesota (1989); available from University Microfilms, Ann Arbor, MI.

Batch, G. L., "Analysis and Optimization of Heater Placement in a Pultrusion Die," Conf. Compos. Inst. Soc. Plast. Ind., 7-C (1990a).

Batch, G. L., and C. W. Macosko, "Kinetic Model for Crosslinking Free Radical Polymerization Including Diffusion Limitations," *J. Appl. Poly. Sci.*, **44**, 1711 (1992).

Batch, G. L., "Analysis of Pultrusion Pressure, Pulling Force, Warp, and Sloughing," Soc. Manufacturing Eng., Manufacturing Methods of Pultrusion, Los Angeles (May 9, 1990c).

Batch, G. L., and C. W. Macosko, "Oxygen Inhibition in Differential Scanning Calorimetry of Free Radical Polymerization," *Thermochimica Acta*, **166**, 185 (1990d).

Buck, H. J., L. T. Blankenship, and P. C. Bryan, "An Optimal Curing Approach for Pultruded Vinyl Ester Parts," Conf. Compos. Inst., Soc. Plastics Ind., 4-C (Feb., 1989).

Byrne, G. D., and A. C. Hindmarsh, "Experiments in Numerical Methods for a Problem of Combustion Modeling," *Appl. Num. Math.*, **1**, 29 (1985).

Faulkner, R., "Reaction Wave Polymerization: Applicability to Reactive Polymer Processing," *Poly. Proc. Eng.*, **3**, 113 (1985).

Goldsworthy, W. B., "Pultrusion—A Growing Tonnage Market for Reinforced Plastics End Products," *Reinf. Plast.* (June, 1971); "Continuous Manufacturing Processes," *Handbook of Composites*, G. Lubin, ed., Van Nostrand Reinhold, New York, p. 479 (1982).

Gonzalez-Romero, V. M., "Studies of Reactive Polymer Processing with Fiberglass Reinforcement," PhD Thesis, Univ. of Minnesota (1983); available from University Microfilms, Ann Arbor, MI.

Gonzalez, V. M., and C. W. Macosko, "Viscosity Rise during Free Radical Crosslinking Polymerization with Inhibition," *J. Rheol.*, **29**, 259 (1985).

Gorthala, R., J. A. Roux, J. G. Vaughan, and R. P. Donti, "Comparison of Processing Parameters for Pultruded Graphite/Epoxy and Fiberglass/Epoxy: A Heat Transfer and Cure Model," Conf. Compos. Inst., Soc. Plast. Ind., 2-A (Feb., 1992).

Gupta, G. K., R. Sacks-Davis, and P. E. Tischer, "A Review of Recent Developments in Solving ODE's," *Comput. Surveys*, **17**, 5 (1985).

Han, C. D., and H. B. Chin, "Development of a Mathematical Model for the Pultrusion of Unsaturated Polyester Resin," *Poly. Eng. Sci.*, **28**(5), 321 (1988).

Jones, B. H., "Pultruding Filamentary Composites—an Experimental and Analytical Determination of Process Parameters," Conf. Reinf. Plast./Compos. Inst., Soc. Plast. Ind. (1974).

Kamal, M. R., and M. E. Ryan, "The Behavior of Thermosetting Compounds in Injection Molding Cavities," *Poly. Eng. Sci.*, **20**(13), 859 (1980).

Langan, L. J., "The Modeling and Control of the Pultrusion Composite Manufacturing Process," MS Thesis, MIT (1986).

Lapidus, L., and G. F. Pinder, *Numerical Solution of Partial Differential Equations in Science and Engineering*, Wiley, New York (1982).

Larock, J. A., H. T. Hahn, and D. J. Evans, "Pultrusion Processes for Thermoplastic Composites," Conf. Compos. Inst., Soc. Plast. Ind., 8-A (Feb., 1989).

Lee, L. J., "Curing of Compression Molded Sheet Molding Compound," *Poly. Eng. Sci.*, **21**, 483 (1981).

Lubin, G., *Handbook of Composites*, Van Nostrand Reinhold, New York (1982).

Ma, C.-C. M., K.-Y. Lee, Y.-D. Lee, and J.-S. Hwang, "The Correlations of Processing Variables for Optimizing the Pultrusion Process," *SAMPE J.*, **22**(5), 42 (1986).

Meyer, R. M., *Handbook of Pultrusion Technology*, Chapman and Hall, New York (1985).

Mijovic, J., and H. T. Wang, "Modeling of Processing of Composites Part II—Temperature Distribution During Cure," *SAMPE J.*, **24**(2), 42 (1988).

Ng, H., and I. Manas-Zloczower, "Kinetic Studies of a Composite Thermoset Cure Reaction—Application in Pultrusion Simulations," *Poly. Eng. Sci.*, **29**, 302 (1989).

Orfeuil, M., *Electric Process Heating*, Battelle Press, Columbus, OH (1987).

Osinski, J. S., L. T. Manzione, and C. Chan, "Thermal Runaway in Fast Polymerization Reactions," *Poly. Proc. Eng.*, **3**, 97 (1985).

Ott, H.-J., "Thermal Conductivity of Composite Materials," *Plast. Rubber Proc. Appl.*, **1**, 9 (1981).

Perry, R. H., and C. H. Chilton, eds., *Chemical Engineers' Handbook*, 5th ed., McGraw-Hill, New York (1973).

Price, H. L., "Curing and Flow of Thermosetting Resins for Composite Material Pultrusion," PhD Thesis, Old Dominion Univ. (1979).

Progelhof, R. C., J. L. Throne, and R. R. Ruetsch, "Methods for Predicting the Thermal Conductivity of Composite Systems: A Review," *Poly. Eng. Sci.*, **16**, 615 (1976).

Pusatcioglu, S. Y., A. L. Fricke, and J. C. Hassler, "Variation of Thermal Conductivity and Specific Heat During Cure of Thermoset Polyesters," *J. Appl. Poly. Sci.*, **24**, 947 (1979).
Roy, R. V., "Pultrusion Modeling for Die Design and Process Control," PhD Thesis, Tufts Univ. (1986); available from University Microfilms, Ann Arbor, MI.
Shampine, L. F., "Measuring Stiffness," *Appl. Num. Math.*, **1**, 107 (1985).
Shampine, L. F., and C. W. Gear, "A User's View of Solving Stiff Ordinary Differential Equations," *SIAM Rev.*, **21**, 1 (1979).
Stevenson, J. F., "Free Radical Polymerization Models for Simulating Reactive Processing," *Poly. Eng. Sci.*, **26**(11), 746 (1986).
Sumerak, J. E., "Understanding Pultrusion Process Variables," *Modern Plastics*, p. 58 (1985); Conf., Reinf. Plast./Compos. Inst., Soc. Plast. Ind. (1985).
Sumerak, J. E., and J. D Martin, "Applying Internal Temperature Measurement Data to Pultrusion Process Control," Conf. Reinf. Plast./Compos. Inst., Soc. Plast. Ind., 1-B (1985).
Trivisano, A., A. Maffezzoli, J. M. Kenny, and L. Nicolais, "Mathematical Modeling of the Pultrusion of Epoxy Based Composites," *Adv. Poly. Techn.*, **10**, 251 (1990).
Tulig, T. J., "A Heat Transfer and Reaction Model for Pultrusion," AIChE Meeting, Chicago (Nov., 1985).
Walsh, S. M., and M. Charmchi, "Heat Transfer Characteristics of a Pultrusion Process," Heat Transf. Conf., Houston (July, 1988).
Walsh, S. M., and N. J. Tessier, "Comparison of Analytical and Experimental Data for the Pultrusion Process," Int. SAMPE Symp., p. 1433 (Mar. 7-10, 1988).
Weast, R. C., ed., *Handbook of Chemistry and Physics*, 58th ed., CRC Press, West Palm Beach (1978).
Yang, Y. S., and L. J. Lee, "Rheokinetic Studies of Unsaturated Polyester Resins," *Poly. Proc. Eng.*, **5**, 327 (1988).

Appendix A: Finite Difference Formulation of Model

Equation 9 is solved by the finite difference method (FDM) (Byrne and Hindmarsh, 1985) using 21 nodes between the centerline and the wall. Time steps were solved implicitly using the Crank-Nicolson method as follows:

$$T_{i,t+\Delta t}=T_{i,t}+\frac{\vartheta_t \Delta t}{2}\left(K_{i,t}+K_{i,t+\Delta t}\right)+\Delta T_{ad}\left(X_{i,t+\Delta t}-X_{i,t}\right)+P_t \Delta t \quad \text{(A1)}$$

where P_t is the time-averaged preheater power from time t to $t+\Delta t$ and K is the rate of heat conduction.

$$K_{i,t}\equiv \alpha_{th}\frac{\partial^2 T}{\partial x^2}+\alpha_{th}\frac{G}{x}\frac{\partial T}{\partial x}$$

The thermal properties are allowed to change with temperature and degree of cure, so K is calculated using the thermal diffusivities averaged between neighboring nodes (east and west) to satisfy the conservation of energy:

$$K_{i,t}=\frac{\alpha_e(\partial T/\partial x)_e-\alpha_w(\partial T/\partial x)_w}{x_e-x_w}+\alpha_{avg}\frac{G}{x_i}\frac{(\partial T/\partial x)_e+(\partial T/\partial x)_w}{2}$$

which for uniformly spaced nodes simplifies as follows:

$$K_{i,t}=\frac{\alpha_e}{(\Delta x)^2}\left(T_{i+1,t}-T_{i,t}\right)-\frac{\alpha_w}{(\Delta x)^2}\left(T_{i,t}-T_{i-1,t}\right)+\frac{\alpha_{avg}G}{2x_i\Delta x}\left(T_{i+1,t}-T_{i-1,t}\right) \quad \text{(A2)}$$

where

$$\alpha_e=\frac{2}{\rho_i C_i}\left[\frac{1}{k_i}+\frac{1}{k_{i+1}}\right]^{-1}$$

$$\alpha_w=\frac{2}{\rho_i C_i}\left[\frac{1}{k_i}+\frac{1}{k_{i-1}}\right]^{-1}$$

$$\alpha_{avg}=\frac{4}{\rho_i C_i}\left[\frac{1}{k_{i-1}}+\frac{2}{k_i}+\frac{1}{k_{i+1}}\right]^{-1}$$

To apply the symmetry boundary condition, Lapidus and Pinder (1982, p. 200) show that the Laplacian operator of equation simplifies at $x=0$ to become:

$$\lim_{x\to 0}\left[\frac{\partial^2 T}{\partial x^2}+\frac{G}{x}\frac{\partial T}{\partial x}\right]=(1+G)\frac{\partial^2 T}{\partial x^2}$$

and hence Eq. A2 reduces at the center node ($i=1$) as follows:

$$K_{1,t}\equiv=\frac{2(1+G)\alpha_e}{(\Delta x)^2}\left(T_{2,t}-T_{1,t}\right) \quad \text{(A3)}$$

At the wall ($i=N$), the convection boundary condition is solved together with the energy balance by replacing the first term of Eq. A2 with the following approximation:

$$\alpha_e(\partial T/\partial x)_e=-\frac{\alpha_w \mathrm{Nu}(S)}{B}\left(T_{N,t}-T_{\mathrm{die},t}\right)$$

$$\alpha_{avg}\frac{G}{x_i}\frac{(\partial T/\partial x)_e+(\partial T/\partial x)_w}{2}=\frac{\alpha_w G}{B}\frac{T_{N,t}-T_{N-1,t}}{\Delta x}$$

$$x_e-x_w=\frac{\Delta x}{2}$$

hence, Eq. A2 becomes:

$$K_{N,t}=\frac{2\alpha_w}{\Delta x}\left[\frac{Nu(S)}{B}\left(T_{\mathrm{die},t}-T_{N,t}\right)-\frac{T_{N,t}-T_{N-1,t}}{\Delta x}\right]+\frac{\alpha_w G}{B\Delta x}\left(T_{N,t}-T_{N-1,t}\right) \quad \text{(A4)}$$

The equations for reaction kinetics (Eqs. 10-13) are also integrated by the Crank-Nicolson technique, and conversion and temperature are solved iteratively, as shown in Figure A1. The equations for reaction and temperature are solved iteratively, and convergence is defined when the *maximum* iteration update for any node is less than E_x for the reaction loop and less than E_T for the temperature loop. This iterative technique allows tridiagonal matrix inversion for temperature, significantly increasing computational speed without affecting accuracy. Whereas previous works which simultaneously solved reaction and temperature equations were performed on a supercomputer (Batch and Macosko, 1987), the decoupled formulation discussed above was able to run on a microcomputer within several minutes (Batch, 1988). This is considered important, because supercomputers are not available to many

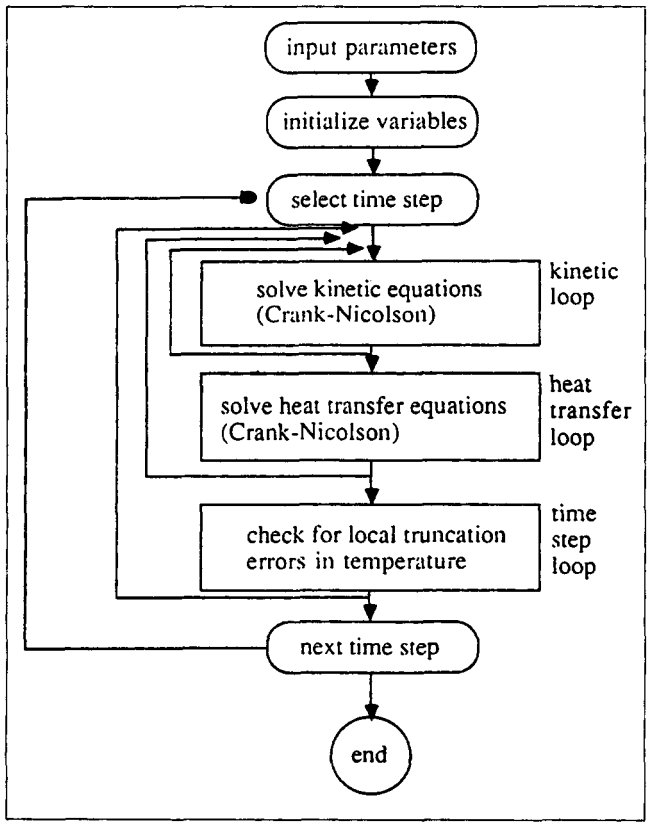

Figure A1. Iterative method for solving transient equations of reaction kinetics and heat transfer.

pultrusion manufacturers who may use predictive software.

Truncation errors are reduced by using a "stiff" variable time step method to improve computational efficiency (Shampine, 1985; Shampine and Gear, 1979; Gupta et al., 1985). Before reaction, profile temperature increases slowly (~1°C/s), hence Δt can be large without significant truncation error. During the reaction exotherm, however, temperature increases much more rapidly (up to 30°C/s), hence time steps are reduced to improve accuracy. Each new time step $\Delta t^{(n+1)}$ is determined from the maximum local truncation error:

$$\Delta t^{(n+1)} = \Delta t^{(n)} \frac{\epsilon_{\text{toler}}}{\max\limits_{\text{all } i} |\epsilon_{i,t}|} \tag{A5}$$

where $\epsilon_{i,t}$ is determined from the previous two time steps:

$$\epsilon_{i,t} \equiv \frac{\Delta t^{(n)}}{12} \frac{\partial^2 f}{\partial t^2} = \frac{\Delta t^{(n)}}{12} \frac{2}{\Delta t^{(n)} + \Delta t^{(n-1)}} \left[\frac{f_{i,t+\Delta t} - f_{i,t}}{\Delta t^{(n)}} - \frac{f_{i,t} - f_{i,t-\Delta t}}{\Delta t^{(n-1)}} \right]$$

and f is the righthand side of Eq. 9:

$$f_{i,t} \equiv K_{i,t} + \Delta T_{\text{ad}} \frac{\partial X}{\partial t} + P$$

To improve stability, Eq. A5 is constrained by both upper and lower time step limits:

$$\Delta t_{\min} \leq \Delta t^{(n+1)} \leq \Delta t_{\max} \tag{A6}$$

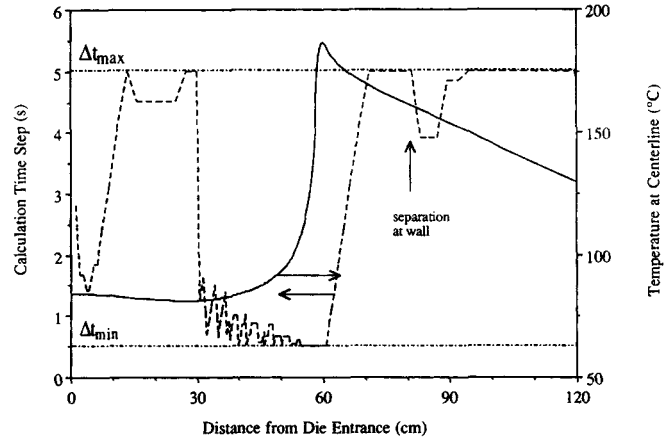

Figure A2. Changes in time step increments in run 1 to minimize truncation errors during the reaction exotherm.

and by the ratio of the change in step size:

$$\frac{1}{R} \leq \frac{\Delta t^{(n+1)}}{\Delta t^{(n)}} \leq R \tag{A7}$$

The size of the time steps and the centerline temperature are in Figure A2. Time steps decrease at the die entrance due to rapid conduction to the wall, but then they increase to nearly their upper limit (5 s) during subsequent heating. Once polymerization begins at the wall, the time steps decrease again and eventually reach the lower limit (0.5 s) when temperature rises fastest at the center. After the cure is complete, the time steps increase again to their upper limit for the duration of the analysis. By using a variable time step procedure, the number of time steps in Figure A2 is reduced from 480 (for a fixed time step of 0.5 s) to 148, thereby reducing run time by 75%.

Appendix B: Accuracy of Numerical Solution

Truncation errors

The analysis was repeated by 1) changing the number of nodes and 2) changing the maximum time increment $\Delta t_{\max}$. In all cases, the temperature predictions were in good agreement with results using N and $\Delta t_{\max}$ from Table 3, indicating that truncation errors were not significant.

Axial conduction errors

Axial conduction is neglected in the model because the Peclet number is very large:

$$Pe \equiv \frac{v}{\alpha_z} L \tag{B1}$$

For the conditions in run 1, L is 121 cm, v is 0.5 cm/s, and α_z (axial thermal diffusivity) is assumed to be 0.02 cm^2/s (three times the transverse thermal diffusivity), and hence Pe is 3,000. However, axial temperature gradients *locally* may be substantially larger than transverse gradients, as illustrated by a local Peclet number defined as follows:

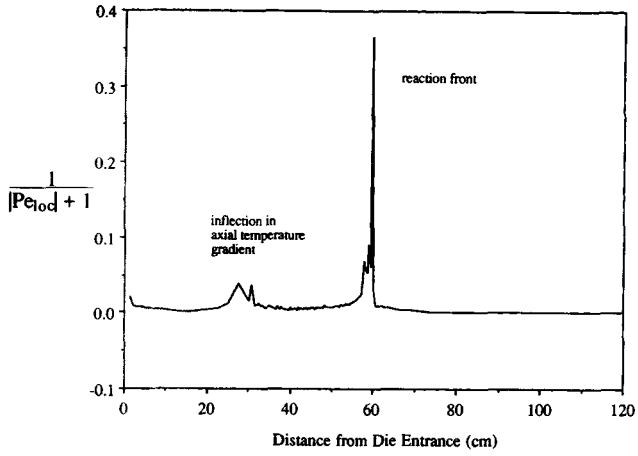

Figure B1. Test for axial conduction in run 1 in the center of the profile.

$$Pe_{loc} \equiv \frac{v}{\alpha_z} \frac{dT/dz}{d^2T/dx^2} \tag{B2}$$

Temperature predictions which neglect axial conduction can be used *a posteriori* to evaluate Pe_{loc}. Figure B1 shows that Pe_{loc} reaches a minimum of 1.7 at the reaction front, hence axial conduction is indeed important over that small portion of the die. Yet, for the bulk of the die length, Pe_{loc} is much larger than unity and axial conduction can be safely neglected.

Frictional heating at wall

Because energy from the puller is performing frictional work at the die, one should consider how much heating can occur at the profile surface. A simple energy balance around a profile perimeter can determine the temperature rise dT for a pulling force F over a distance dz under adiabatic conditions, that is, where heat conduction to either the die metal or profile is neglected:

$$V\rho C dT = F_{frict}\, dz = P A \mu_f dz \tag{B3}$$

or by integrating,

$$\Delta T_{frict} = \frac{A}{V\rho C}\int_0^L P\mu_f dz = \frac{LF}{V\rho C} \tag{B4}$$

where V, A, and Z are the volume, surface area, and perimeter of the control volume, respectively, μ_f is friction coefficient, P is internal pressure, and F is pulling force given as follows:

$$F = Z\int_0^L P\mu_f dz = \frac{A}{L}\int_0^L P\mu_f dz \tag{B5}$$

For a control volume of thickness h on the perimeter of a 1-in. (25-mm) round profile, the area to volume ratio is:

$$\frac{L}{V} = \frac{L}{\pi L[R^2 - (R-h)^2]} = \frac{1}{\pi R^2[1-(1-h/R)^2]} \tag{B6}$$

where h can be given as the characteristic heat conduction thickness during frictional heating based on the residence time t_{res}, $h = \sqrt{t_{res}\alpha_{th}}$.

As a worse case, we can assume that most of the pulling force occurs over a short distance inside the die where the liquid to solid transition takes place on the profile surface (Batch, 1989). For $\alpha_{th} = 0.0035$ cm^2/s, $t_{res} = t_{die}/10 = 24$ s, $R = 1.27$ cm, and $F = 2{,}220$ N [or about 500 lb (230 kg)], then h is 0.29 cm and ΔT_{frict} is 6.0°C. It is difficult to say whether a temperature increase of 6°C at the wall would create a significant change in overall curing rate. Modeling of frictional heating requires a coupled analysis of pulling force and heat transfer.

Manuscript received Aug. 30, 1991, and revision received Dec. 14, 1992.